Neutrino-Nucleus Interactions

Authors:

*H. Gallagher, Tufts University, hugh.gallagher@tufts.edu

G. Garvey, Los Alamos National Laboratory, garvey@lanl.gov

G. Zeller, Fermi National Accelerator Laboratory, gzeller@fnal.gov

Prepared for the *Annual Review of Nuclear and Particle Science*

*) Corresponding Author contact information: Tufts University, Sci-Tech Center, 4 Colby St, Medford, MA 02155

1) Introduction

Over the past decade, the discovery and study of neutrino oscillations has renewed interest in neutrino-nucleus interactions. Such interactions readily separate into three distinct topical areas that can be classified as low, medium, and high energy. At low energy O(MeV), the wave-length scale of the interaction is greater than the nuclear diameter so that the initial and final states are specific nuclear levels. These are the interactions of most interest to solar and reactor neutrino oscillation experiments. In the medium energy regime O(1 GeV), which constitutes the bulk of this review, the interaction length is hadronic ~(1 fm) with important nuclear effects. These are the interactions of most interest to atmospheric and accelerator-based neutrino oscillation experiments. At high energies O(100 GeV), the scale for deep inelastic scattering becomes partonic (~0.1fm) and nuclear effects, though present, are less significant.

This article focuses on medium energy neutrino-nucleus interactions ($\sim 0.3 < E_\nu < 3.0$ GeV) with particular emphasis on quasi-elastic (QE) neutrino scattering, the simplest and most copious interaction at these energies. We restrict our focus for several reasons:

- Future high-statistics oscillation experiments will require a thorough understanding of this region, in particular those that use QE events as their signal sample to investigate neutrino oscillations.

- Although neutrino-nucleon QE scattering is well characterized, when this process occurs within the nucleus, the description becomes more complicated. The complexities exposed here are present in other channels.
- Neutrino-nucleus QE scattering has been the focus of substantial work over the past 40 years, and comparisons of recent results to those from the bubble chamber era reveal differences challenging our assumptions regarding these processes.

In this article we review the standard picture of QE scattering drawing heavily on the analogous electro-nuclear scattering processes, summarize measurements of neutrino QE scattering, and present ideas on additional nuclear effects that may play a role in the interpretation of this data. We conclude with a commentary on future directions.

2. Quasi-Elastic Lepton-Nucleus Scattering: Preliminaries

The simplest description of neutrino-nuclear scattering is built upon two ingredients: a characterization of neutrino-nucleon scattering, and a model for nucleons in the nucleus. For elastic scattering (or what is called QE scattering in the case of charged current neutrino scattering) the former is well established, and the latter has been the subject of much theoretical and experimental work in the context of electron scattering over the past forty years. Figure 1 represents this picture schematically. In the simplest and most

common picture, neutrino-nucleus scattering is treated as the incoherent sum of scattering from free nucleons. This is the so-called "impulse approximation" approach. In reality, the nucleons are not independent particles and, as a result, more complex nuclear dynamics are involved. The extent to which each of these two pictures describes what is observed experimentally will be a focus of this article.

To start we review lepton scattering from free nucleons and summarize information on the weak hadronic current obtained from past experiments. Both are important ingredients in any description of neutrino QE scattering.

2.1 – (Quasi-) Elastic Scattering on Free Nucleons

It is illustrative to start from the case of elastic electron scattering from free nucleons. In this situation the amplitude is:

$$M = \frac{e^2}{q^2}\bar{u}_e(k')\gamma^\mu u_e(k) j_\mu \quad (1)$$

where $e = \sqrt{2\pi\alpha}$, α is the fine structure constant, $u_e(k)$ and $\bar{u}_e(k')$ represent the initial and final states of the electron and j_μ is the hadronic vector current. The hadronic vector current captures the underlying nucleon structure and is written in terms of the well known Dirac and Pauli nucleon vector form factors, $F_1(q)$ and $F_2(q)$, which are functions of a single variable, the magnitude of the three momentum transfer $|\vec{q}| \equiv q$

$$j_\mu(q^2) \sim \bar{u}(p')\left[F_1(q^2)\gamma_\mu + \frac{1}{2M} F_2(q^2)\sigma_{\mu\nu} p_\nu \right] u(p)$$

$$F_1(q^2) = \frac{1}{2}(F_1^S(q^2) + \tau_3 F_1^V(q^2)) \qquad 2MF_2^S(0) = \mu_p' + \mu_n = -0.120$$

$$F_1^S(0) = 1 \qquad F_2^V(0) = 1 \qquad 2MF_2^V(0) = \mu_p' - \mu_n = 3.706 \quad (2)$$

where M is the proton mass and μ_p' and μ_n are the anomalous magnetic moments of the proton and neutron. The superscripts S and V refer to the isoscalar and isovector contributions. The initial and final states of the struck nucleon are shown as u(p) and u(p'), where only the magnitude of the nucleon momentum is explicit, spin and isospin states are suppressed. CVC and isospin conservation allow QE electron scattering (QEES) to establish the vector current contributions of both charged and neutral current scattering of neutrinos.

It proved useful in analyzing electron scattering to separate the scattering yields into longitudinal and transverse contributions. The longitudinal contribution originates from scattering where the polarization of the virtual photon is along the direction of momentum transfer (Coulomb scattering) while for transverse scattering it is perpendicular to the momentum transfer. The differential cross section for electron-nucleon scattering is:

$$\frac{d\sigma}{d\Omega_e} = \sigma_{Mott} \frac{E'}{E_0}\left[\frac{G_E^2(Q^2) + \tau G_M^2(Q^2)}{1+\tau} + 2\tau G_M^2(Q^2)\tan^2\left(\frac{\theta}{2}\right) \right] \quad (3)$$

These form factors are related to the Pauli and Dirac forms via $G_M(Q^2) = F_1(Q^2) + F_2(Q^2)$, $G_E(Q^2) = F_1(Q^2) - \tau F_2(Q^2)$, and $\tau = Q^2/4M^2$. At energies of interest to this review, the transverse response dominates, particularly at large scattering angles.

When considering neutrino scattering from nucleons, an axial current comes into play. The total nucleon current coupling to the charged weak leptonic current is an isovector one body nucleon current with both vector and axial-vector components: $j^{\mu}(Q^2) = j_V^{\mu}(Q^2) + j_A^{\mu}(Q^2)$. The full nucleon weak current had been written down by Llewellyn-Smith (1) but for our purposes it suffices to write the axial current of the nucleon as

$$j_A^{\mu}(Q^2) = \bar{u}(p')\left(G_A(Q^2)\gamma^{\mu} + \frac{1}{2M} G_P(Q^2) q^{\mu} \right)\gamma^5 u(p) \qquad (4)$$

where the induced pseudoscalar $G_P(Q^2)=4m_N^2 G_A/(m_\pi^2+Q^2)$ is determined by PCAC and the axial-vector form factor $G_A(Q^2)$ is established from experiment.

The weak leptonic current is

$$j_{\mu}^{l} = \bar{\psi}_{\substack{l^- \\ l^+}}(1 \mp \gamma_5)\gamma_{\mu}\psi_{\substack{\nu \\ \bar{\nu}}} \qquad (5)$$

The lepton-nucleon coupling is the scalar product of the two currents. The change in sign for the axial coupling arises from the opposite helicity of neutrinos and anti-neutrinos leading to constructive interference between the transverse vector and axial vector amplitudes for neutrino cross sections and destructive interference for anti-neutrinos.

It follows that the differential cross section for neutrino QE scattering off free nucleons can be expressed in the form (1):

$$\frac{d\sigma}{dQ^2} = \frac{G_f^2 M^2 \cos^2\theta_C}{8\pi E_\nu^2}\left[A \mp \frac{(s-u)}{M^2} B + \frac{(s-u)^2}{M^4} C \right] \qquad (6)$$

where (-)+ refers to (anti)neutrino scattering, (s - u) = $4ME_\nu - Q^2 - m^2$, and m is the lepton mass. The factors A, B, and C are functions of the Q^2-dependent vector, axial-vector, and pseudoscalar form factors:

$$
\begin{aligned}
A &= \frac{(m^2+Q^2)}{M^2}\left[(1+\tau)G_A^2 - (1-\tau)F_1^2 + \tau(1-\tau)F_2^2 + 4\tau F_1 F_2 \right. \\
&\quad \left. - \frac{m^2}{4M^2}\left(\left(F_1+F_2\right)^2 + \left(G_A+2G_P\right)^2 - \left(\frac{Q^2}{M^2}+4\right)G_P^2 \right) \right] \\
B &= \frac{Q^2}{M^2} G_A (F_1+F_2) \\
C &= \frac{1}{4}(G_A^2 + F_1^2 + \tau F_2^2)
\end{aligned}
\qquad (7)
$$

and F_1 and F_2 are the aforementioned isovector Dirac and Pauli vector form factors. With the vector form factors determined from electron scattering and small contributions from the pseudoscalar form factor for ν_μ scattering, early studies of neutrino QE scattering focused on investigating the axial-vector form factor of the nucleon.

2.2 – Early Investigations of the Weak Hadronic Current

Some of the earliest experimental investigations of neutrino QE scattering, $\nu_\mu + n \rightarrow \mu^- + p$, were performed in the late 1960's using spark chambers (aluminum, iron) (2,3) and bubble chambers (propane, freon) (4) as neutrino detectors. These early experiments provided the first neutrino QE scattering event samples from which initial determinations of the underlying nucleon form factors were made. In the early 1970's, many experiments

employed simpler targets, such as deuterium (5), recognizing that they provided cleaner measurements less influenced by nuclear effects. The primary focus of these experiments was measuring free nucleon form factors. At the time, these form factors were recognized as an important ingredient in the analysis of neutral currents ($\nu_\mu + p \rightarrow \nu_\mu + p$ and $\bar{\nu}_\mu + p \rightarrow \bar{\nu}_\mu + p$) so careful study of the charged-current component of this reaction began.

Equations [6-7] were typically used to analyze the experimental data on deuterium, subject to minor effects of Fermi motion and Pauli blocking in deuterium. The vector form factors could be determined from electron scattering, thus leaving the neutrino experiments to measure the axial-vector form factor of the nucleon. Traditionally, the axial-vector form factor is assumed to have a dipole form:

$$G_A(Q^2) = \frac{g_A}{\left(1 + Q^2 / M_A^2\right)} \qquad (8)$$

dependent on two empirical parameters: the value of the axial-vector form factor at $Q^2=0$ ($g_A=F_A(0)=1.2671$ determined with high precision from nuclear beta decay (6)) and an axial mass, M_A which must be determined experimentally. Values of M_A ranging from 0.65 to 1.09 GeV were obtained from fitting both the total rate of CCQE events and their measured Q^2 dependence. Refs. (7,8) provide an excellent review of these early experimental M_A determinations. By the end of this period, it was concluded that the neutrino QE cross section could be accurately and consistently described by V-A theory assuming a dipole axial-vector form factor with $M_A=1.026 \pm 0.021$ GeV (9). These conclusions were largely driven by experimental measurements on deuterium, but less-precise data on other heavier targets also contributed (see Table 1). More recently, this

same data has been re-analyzed using modern vector form factors as input. The use of improved non-dipole vector form factors (10) slightly shifts the best-fit axial mass values obtained from this data; however the conclusion is still that $M_A \approx 1.0$ GeV (11,12). These results are consistent with those obtained from the electro-production of pions produced near threshold (9).

3. Quasi-Elastic Electro-Nucleus Scattering

While the focus of early neutrino QE experiments centered on determination of M_A, the process of lepton-nucleus quasi-elastic scattering was far more thoroughly studied with electrons. The fact that electron beams have precisely known energies ($\Delta E/E < 10^{-3}$) and fluxes (1%) and the momentum of the scattered electrons can be measured with comparable resolution (by a magnetic spectrometer at fixed scattering angle) means the energy and momentum transferred to the nucleus in the collision are precisely measured. Large sets of inclusive scattering data on a variety of nuclei at varying kinematics have been collected by experiments at SLAC, Bates, Saclay, Mainz, and JLab over the past forty years (31). There is an excellent recent review (32) of the status of inclusive quasi-elastic electron scattering (QEES) from nuclei. We draw heavily on that review in the brief summary given below. A detailed presentation of the theoretical formalism employed in QEES can be found in Reference (33).

Figure 2 shows an idealized inclusive spectrum resulting from a few GeV electron beam scattered from a nuclear target (32). The large peak just below 400 MeV corresponds to

the elastic scattering of electrons off individual nucleons. The center of the peak corresponds roughly to the kinetic energy transferred to a single nucleon initially at rest in the lab frame, the width of the peak results from the nucleon's Fermi momentum in the target nucleus. The kinetic energy acquired by the nucleon is given non-relativistically by $\omega \sim (\vec{p}_i + \vec{q})^2 / 2m_N$ where $\vec{p}_i$ is the nucleon's Fermi momentum, $\vec{q}$ the momentum transferred in the collision, and m_N the nucleon mass. This is the paradigm for all QE scattering in the impulse approximation, the cross section is an incoherent sum of the scattering off individual nucleons with the recoiling nucleus carrying off momentum $-\vec{p}_i$ and energy $p_i^2 / 2(A-1)m_N + E_h$. E_h is the energy of hole created in the recoiling A-1 nucleus (occasionally referred to as the 'binding or separation energy of the struck nucleon). Also shown in Figure 2 are yields of scattered electrons occurring at higher ω due to pion creation, delta formation or deep inelastic scattering.

It is useful to briefly examine the formalism used in the analysis of electro-nuclear scattering as it is carried over to neutrino-nucleus scattering. Introducing the notation $Q^2 = -(p_0 - p')^2 = -q^2 = |\vec{q}|^2 - \omega^2$, the electro-nuclear cross section as function of solid angle (θ) and energy loss (ω) is written in terms of longitudinal $R_L(q,\omega)$ and transverse $R_T(q,\omega)$ response functions,

$$\frac{d\sigma^2}{d\Omega_e d\omega} = \left(\frac{d\sigma}{d\Omega_e}\right)_{Mott} \left\{ \left(\frac{Q}{|\vec{q}|}\right)^4 R_L(|\vec{q}|,\omega) + \left(\frac{1}{2}\left(\frac{Q}{|\vec{q}|}\right)^2 + \tan^2\frac{\theta}{2} \right) R_T(|\vec{q}|,\omega) \right\} \quad (9)$$

$(d\sigma / d\Omega_e)_{Mott} = \alpha^2 \cos^2(\theta/2) / E \sin^4(\theta/2)$. For QE scattering from individual nucleons, the response functions are written in terms of Dirac and Pauli nucleon vector form

factors $F_1(q)$ and $F_2(q)$ mentioned previously. To apply the concept of QE scattering, $|\vec{q}|$ should be ≥ 0.3 GeV/c to resolve a single nucleon within the nucleus.

Early implementation (34-36) of this approach was carried out with an appealing contact (37) with experiment. The nucleus was treated as a Fermi gas, with just two parameters, the Fermi momentum k_F and a "separation" energy ($\sim E_h$). Qualitative agreement was achieved with data and the parameters k_F and E_h determined for a range of nuclei showed systematic and expected behavior. However quantitative agreement with measured cross sections was only at the tens of % level.

Over time many experimental and theoretical advances were made. A uniform density Fermi gas approximation was improved by use of a local density approximation (38) that more realistically reflects the nucleon momentum distribution in nuclei. This approach adds to the independent particle distribution a term with higher nucleon momentum and separation energy (38) to account for the effect of short-range nucleon-nucleon correlations. This information is compactly but incompletely incorporated in a nuclear spectral function, $S(\vec{p},E)$, which gives the probability of finding a nucleon with momentum $\vec{p}$ and removal energy E. The important role of nucleon-nucleon correlations will be addressed in Section 5.

The collection of large amounts of inclusive QE data at varying incident energies and scattering angles allowed a very important scaling property to be uncovered (39). A simple

version of scaling sufficient for this review is presented below but there are many further refinements in the literature (32).

Figure 3a shows the inclusive electron scattering cross section off ^{3}He at differing incident energies and scattering angles. The greatly varying values of the cross sections can be related by employing a scaling variable y, related to the scaling variable $x=Q^2/2M\omega$ used in deep inelastic scattering. y is obtained assuming that the scattering occurs off a single nucleon.

The energy transferred from the electron to the nucleus is ω. In the case of QE scattering the energy transferred, ω, is given by $\omega=T_n+E_s+E_{recoil}$, where T_n is the kinetic energy given to the struck nucleon, E_s is the energy of the "hole" in the residual A-1 system and E_{recoil} is the recoil kinetic energy of the A-1 system. The recoil's momentum is $-\vec{k}$ and the final momentum of the struck nucleon is $\vec{k}+\vec{q}$. Thus

$$\begin{aligned}\omega &= \left[(\vec{k}+\vec{q})^2+m^2\right]^{1/2} - m + E_s + E_{recoil} \\ &= \left[k_{\|}^2 + 2k_{\|}q + q^2 + k_{\perp}^2 + m^2\right]^{1/2} - m + E_s + E_{recoil}\end{aligned} \qquad (10)$$

where $k_{\|}$ and $k_{\perp}$ are the momentum parallel and perpendicular to the direction of the transferred momentum. In the limit of very large q,

$$k_{\|} = (\omega^2 + 2\omega m)^{\frac{1}{2}} - q \qquad (11)$$

In this situation ω and q are not independent and a scaling variable $y=k_{//}$ is suggested. The scaling function $F(y,q)$ is defined as

$$F(y,q) = \frac{d^2\sigma}{d\Omega d\omega}\left(\frac{1}{Z\sigma_{ep}(q) + N\sigma_{en}(q)}\right)\frac{d\omega}{dy} \qquad (12)$$

where the contribution to the inclusive QEES nuclear cross section of Z protons and N neutrons at 3 momentum transfer $|\vec{q}| \equiv q$ is divided out. Figure 3b shows the data from Fig. 3a as *F(y)* as function of y. The collapse of the data for values of y ≤0 is startling. The value y=0 corresponds to $\omega=Q^2/2m=(q^2-\omega^2)/2m$, the kinematics of scattering off a free nucleon at rest. The existence such scaling establishes some essential facts; the bound nucleon form factors are not modified from their free value to within 3% (40) and the mass of the bound nucleon can to be taken as its free value. The marked deviation from scaling above y=0 is variously attributed to short range correlations, meson exchange currents, pion production, and the low ω tail of the Δ resonance; some of which are suggested in Figure 2. Thus it is clear that QE scattering does occur but other processes come into play.

A relativistic formulation of the Fermi Gas (RFG) (41) expands the kinematic range of the model and shows y scaling to hold in the limit $|\vec{q}| \to \infty$. This approach quite naturally led to the concept of super-scaling (42) that applies a modified form of y scaling to all nuclei. In this approach a dimensionless scaling variable ψ is employed where

$$\psi = \frac{y_{RFG}}{k_F} = \frac{m_N}{k_F}\left(\lambda\sqrt{1+\tau^{-1}} - \kappa\right) \qquad (13)$$

with $\kappa = q/2m_N$, $\lambda = \omega/2m_N$ and $\tau = Q^2/4m_N^2$. It was further shown that super-scaling holds for nuclei with A ≥ 12 (42). It appears to work to ± 20% for all values of *q* and A ≥ 12. Holding the energy and scattering angle constant, the scaling between different A for y'<0

holds to better than 5%. This is a consequence of the approximately constant density of nuclear matter, where the slight increase of k_F with A accounts for the reduced surface to volume ratio with increasing A. Thus rather than trying to use a model for the momentum and separation energy of nucleons in a nucleus one could use an appropriate scaling function $F(\psi,q)$.

As indicated earlier, with extensive data at various energies and scattering angles the electro-nuclear QEES can be separated into longitudinal and transverse components and their scaling separately investigated. It was found that the longitudinal response scales for all values of y (43) and is of the expected magnitude (i.e., satisfies the Coulomb sum rule) (42,43) while the transverse response diverges seriously above ψ=0 and is appreciably larger than predicted (42) in the relativistic Fermi Gas model. Thus, to use QEES to establish a best spectral function, $S(\vec{p},E)$, the most reliable information would come from $F_L(\psi,q)$ (43) as it is free of the effects that complicate $F_T(\psi,q)$ (i.e. meson exchange currents, low energy tail of the delta). However there are significant dynamical effects in the transverse response that are not captured in the impulse approximation.

The experience obtained in QEES is directly transferable to neutrino-nucleus charged-current quasi-elastic scattering (CCQE). The one body nucleon vector current (Eq. 2) employed in QEES is modified to the nucleon's weak vector-axial one body current (Eq. 4). An important aspect of this modification results from the opposite helicity of neutrinos and anti-neutrinos (Eq. 5) requiring the interference between the transverse vector amplitude and the axial vector amplitude be constructive for neutrino CCQE and destructive for antineutrino CCQE. Many groups have

published extensively on neutrino-nucleus CCQE and useful expressions for the neutrino-nucleus CCQE cross sections can be found in many articles (44-48). It is important to note that all published calculations of CCQE based on the impulse approximation are in close agreement. The formulation in (44) is quite complete and additionally has a useful discussion of results of this formalism. Ref (46) explicitly deals with final state interactions (FSI) which are of great importance in identifying the specific neutrino-nucleus interaction creating the charged lepton. As FSI played a minor role in inclusive QEES most authors did not include their effects. Experimenters are well advised to acquaint themselves with the effects of FSI as presented in (46). We will discuss this further in the following section.

The next section will present the result of CCQE scattering experiments and compare them to the theory presented above.

4. Experimental Aspects of Neutrino-Nucleus Quasi-Elastic Scattering

We now turn our attention to recent results on neutrino QE scattering from nuclei. We provide a reasonably comprehensive review, not only of the final results, but of the underlying experimental techniques and assumptions. This will include a discussion of detector technologies, event selection, kinematic reconstruction, flux determination, and important backgrounds.

4.1 – The Renaissance of Neutrino Interaction Physics

By the late 1990's, focus had shifted from the study of neutral currents and the basic properties of neutrino interactions to the investigation of neutrino oscillations. The discovery of neutrino oscillation brought with it more intense neutrino beams and large electronic detectors largely composed of water, iron, or mineral oil. Table 1 summarizes the experimental studies of neutrino QE scattering in the oscillation era including new experiments that are expected to collect data in the near future.

So far, axial mass values ranging from M_A =1.05 to 1.35 GeV have been obtained from modern data, with many of the experiments systematically measuring higher M_A values than those obtained from the deuterium data. This has created some interesting questions. First, it is first instructive to compare the various experimental techniques.

4.2 – Experimental Analyses

Table 2 summarizes the various experimental techniques that have been employed in the study of neutrino and antineutrino QE events as well as the results that have been obtained from these samples.

4.2.1 – Quasi-Elastic Event Selection and Detector Technology

The criteria used to select QE events is strongly influenced by both the target material and the detector technology. The various detectors and selection techniques that have been used to isolate neutrino QE events can be grouped into three main categories: bubble chambers, tracking detectors, and Cerenkov detectors.

Because of their low energy thresholds for protons (typically, $\geq\sim 100-200$ MeV/c in momentum) and deuterium fills, bubble chambers (ANL, BEBC, BNL, FNAL GGM, SKAT) typically had sample purities that impressively range from 97%-99%. Event selection is robust and is based on the identification of three final state tracks, one each from the muon, proton, and spectator proton in the QE scattering event: $\nu_\mu d \rightarrow \mu^- p p_s$. Both 'three-track' and 'two-track' (where the spectator proton is not identified) were used. The situation is, of course, different for the case of antineutrino QE scattering: $\bar{\nu}_\mu d \rightarrow \mu^+ n n_s$. Here, the QE event selection is based on the identification of a single track (the μ^+) as the final state neutron is typically not reconstructed. As a result, antineutrino QE purities are typically lower, ranging from 75-85%. In either case, the lowest Q^2 region was often excluded in the analysis of these data in order to avoid regions with poor identification efficiency, nuclear effects, and larger backgrounds.

The analysis strategy of modern experiments remains largely unchanged from the bubble chamber era. From the sample of collected events, those identified as QE are selected and measured. If the scattering is truly QE, then the neutrino energy and Q^2 can both be estimated from the outgoing lepton energy and scattering angle. In many analyses, this

method is used for all events in the 'quasi-elastic-like' sample. This will produce a bias in the measurement due to the presence of background events in this category, so one has to be confident that the background (both normalization and kinematic distributions) are being modeled. The nuclear-model dependence of kinematic reconstruction of this type has been evaluated in Reference (54). In this case, the efficiency and purity of the QE selection are strongly affected by the capabilities of the detector.

Since most experiments built during the modern era were primarily designed for neutrino oscillation measurements, statistics were at a premium. For this reason, experiments employed heavy targets as their neutrino detectors and a variety of different detector technologies. These experiments fall into two broad categories: tracking and Cerenkov detectors.

Tracking experiments attempt to identify each charged particle in an event as it traverses active elements of the detector, typically drift chambers or segmented scintillation elements, while Čerenkov experiments use large tanks of water or mineral oil as a target with photodetectors lining the inner surface of the tank to collect light emitted by relativistic charged particles. In the latter case, the final state proton emitted in neutrino QE interactions is typically below Cerenkov threshold and hence undetected. In tracking and Čerenkov detectors, timing resolutions on the O(10 ns) are also often used to detect the presence or absence of a decay for particle identification. As an example, the QE selection in the MiniBooNE Cerenkov detector requires a final state muon and a single delayed decay electron.

For tracking detectors, the detection thresholds for recoil protons plays a significant role. Studies of neutrino QE event samples have included the analysis of both 1-track (muon + no proton) and 2-track (muon + proton) event samples. Note that such 1-track samples were never considered in bubble chamber experiments, except of course in the case of antineutrino scattering. As in the case of the bubble chamber detectors, antineutrino QE events are identified based solely on the outgoing muon from 1-track samples. Typical QE purities in these detectors range from 60-70%.

Looking at Table 2, some trends are immediately apparent. First, the event selection that defines the "quasi-elastic" sample varies from experiment to experiment. Second, much larger event samples have become available in the modern era. Third, sample purities have are typically lower in the modern era. We will discuss why that is the case in the next section.

4.2.2 – Nuclear Effects, Inefficiencies, and Backgrounds

All QE analyses are subject to some level of background contamination. Nuclear effects play a large role both in the estimation and removal of background events from such samples. They can also contribute a source of inefficiency in the selection of QE events.

The first step in the analysis, the selection of QE events, brings us squarely into the realm of nuclear physics. The fundamental process we seek to measure, $\nu_\mu n \to \mu^- p$ in the case of neutrinos and $\bar{\nu}_\mu p \to \mu^+ n$ in the case of antineutrinos, is occurring in a nuclear

environment and our event selection is based on what is visible in the detector after intranuclear processes have already occurred. Events can both fail to make it into the sample or be spuriously selected. QE events that fail to make it into the sample contribute a source of inefficiency, while non-QE events that spuriously make it into the sample provide a source of background.

The largest sources of background contamination and inefficiency stem from nuclear effects associated with final state interactions (FSI). FSI generically refer to the re-scattering of hadrons produced in the intial neutrino interaction before they have had a chance to exit the target nucleus. Final state effects lead to topological changes in the final state that can impact both signal and background processes. For example, QE interactions can evade the experimental selection due to multi-nucleon knock-out and nucleon rescattering which both increase the number of nucleons emitted and lower their energies. Selection techniques relying on the identification of a final state proton can be especially susceptible to such effects. At the same time, events from non-QE interactions can enter the sample by mimicking a QE signature. The predominant source of such backgrounds are charged-current pion production channels, in particular, in the case that the pion is absorbed in the target nucleus. Estimates of single pion backgrounds are typically made from some combination of simulations and data-driven methods incorporating additional events samples, and have historically had large (>10%) uncertainties associated with them. The fact that modern experiments use heavy nuclear targets (where such effects are large) and cannot rely on the identification of the full interaction (muon + proton + spectator) are

the main reasons why QE event sample purities are not as high as those achieved in deuterium-filled bubble chambers.

In addition to nuclear effects, there can also be limitations posed by the detector itself (55). The inability to detect low energy particles (particularly nucleons) emerging from the target nucleus or the mis-identification of particles that are observed can also add potential sources of background and require corrections to the analysis of QE data. Such effects vary from detector to detector.

In order to estimate the impact of nuclear physics effects on their analyses the experiments in Table 2 used two common ingredients. For the nuclear model they tended to use some type of Fermi Gas model, perhaps augmented to include a high-momentum tail due to short range correlations (56,57). To estimate the effects of final state interactions, they used intranuclear rescattering simulations (58), which will be described in more detail in Section 5.

4.2.3 – Flux Determination

Central to the extraction of absolute cross sections is a prediction of the incoming neutrino flux. All neutrino experiments measure the rate of interactions in their detector which is a product of the neutrino interaction cross section, the incoming neutrino flux, and of course, detection efficiencies. Obtaining a reliable estimate of the neutrino flux in a neutrino experiment has been notoriously difficult and remains a challenge.

Conventional accelerator-based neutrino beams are created by directing an intense proton beam onto a compact target (typically beryllium or carbon), focusing the resulting pion/kaons using magnetic devices, and directing the secondaries into an evacuated or low density region where they decay into neutrinos. Such beamlines can also include instrumentation to monitor the intensity and steering of the primary proton beam, the hadron flux, and the flux of downstream muons. A detailed review of neutrino beams can be found in Reference (59).

All neutrino flux predictions start from an estimate of meson production for a particular primary beam energy and target material. Historically, such hadro-production cross sections have not been well-measured and have directly contributed large uncertainties (20%-40% or more) to the attempts by early experiments to extract neutrino QE cross sections from their data. To add to this, early experiments also often observed large (up to x2!) discrepancies between their observed neutrino rates and their starting predictions. Where possible, experiments cross-checked the normalization of their neutrino fluxes using events with well-known cross sections. This was common practice and included using samples of charged-current deep inelastic scattering (DIS) or inverse muon decay (IMD) events to correct flux predictions. Other times, experiments dangerously used their observed ν_μ QE scattering rates to determine their flux normalization. Such a procedure creates an unwanted circularity and should, of course, be strictly avoided in the case where one also wants to use the same data to measure a absolute cross section!

Today, the availability of dedicated hadro-production experiments has increased the precision with which neutrino flux predictions can be made. As a result, use of such external data has become the sole starting point for many modern neutrino cross section measurements. For experiments with higher energy neutrino beams, charged-current DIS and IMD samples remain a viable cross-check on these flux extraction procedures.

4.3 – Experimental Results

With a known neutrino flux, QE events selected, the efficiency of their identification assessed, and backgrounds removed, an experiment can obtain physics results. -Such measurements include a value for M_A from the observed Q^2 distribution of the events, the neutrino QE interaction cross section, and differential cross sections. Comparison of modern measurements of these quantities to the theory discussed in Section 3 immediately reveal several discrepancies:

Low Q^2: The first is a suppression of events at low Q^2 (Q^2<0.2 GeV^2) when their Q^2 shape is compared to standard predictions. This effect is best illustrated in the MiniBooNE data because of its high statistics (Figure 4b), but has also been observed in multiple low energy neutrino experiments over the years (7,8). Because neutrino oscillation experiments typically collect a large fraction of their data at low Q^2, discrepancies in this region naturally drew much attention. A first attempt to better describe the experimental data at low Q^2 included rescaling the amount of Pauli blocking in the impulse approximation calculations (25). Although naïve Pauli blocking adjustments were successful, recently

improved modeling of the non-QE backgrounds, which are large in this region, also greatly improve the agreement at low Q^2 (26). Regardless of the chosen remedy, the discrepancy at low Q^2 should not have been surprising given that at these low values of Q^2, the exchanged boson is probing a region significantly larger than a single nucleon, thereby violating one of our assumptions in the impulse approximation models. –As a result, neutrino events at these low Q^2 values are not technically QE in the electron-scattering sense, so some care must be taken in this region.

Q^2 shape: In addition to discrepancies at low Q^2, the overall distribution of the events is also shifted to higher Q^2 values in much of the experimental data (Figure 4b). As a result, this "harder" data spectrum requires a higher M_A value than the prior world average ($M_A \sim 1.0$ GeV) when fit using the form factors and nuclear models described previously. The M_A values determined by MiniBooNE, K2K, and preliminary results from MINOS all show similar trends – harder than expected Q^2 distributions which result in systematically higher than expected M_A values when fit using these models. M_A values determined from these experiments range anywhere from M_A=1.14 to 1.35 GeV (22,25-27). The MINOS result is particularly interesting in that it shows the same trend that is present in carbon and oxygen at ~1 GeV is also present in iron for 1-10 GeV neutrinos (27). There is no physical basis for such an M_A increase other than as a characterization of the harder spectrum experimentally observed. The source of this difference is not fully understood at present.

Quasi-Elastic Cross Section Normalization: Using well-determined neutrino flux predictions, MiniBooNE, and NOMAD have re-measured the QE interaction cross section as a function of neutrino energy, a quantity that was frequently reported in early experiments. All measure cross sections on carbon (Figure 4a), with the results at low energy (E_ν<2 GeV) being the first measurements on a nuclear target at those energies. The resulting neutrino QE cross sections at the lowest energies (26,29) are ~30% larger than predictions made using the impulse approximation with well established parameters (38-41,44,56,60,61). Figure 4a includes several representative calculations including the relativistic Fermi Gas model and the spectral function approach described previously (38,56) which has been very successful at describing electron scattering data over a wide range of kinematics (38). For comparisons to additional models (46,62-64) which yield similar results and predictions for other variables, see Ref. (65).

It is not only surprising that the measured QE cross section at low energy exceeds the well-established impulse approximation calculations, but that **the measured cross section on carbon even appears to exceed that for 6 free neutrons!** This, of course, must be understood. Any attempts to account for this observed yield via the impulse approximation fail as all refinements reduce the predicted cross section below the Fermi Gas approximation which already generates a cross section below 6 free neutrons. To achieve an enhanced cross section, one must naturally introduce correlations. As one example, the black solid line shown in Figure 4a shows the prediction from a non-relativistic model which also allows the computation of multi particle-hole contributions (66). These additions significantly enhance the cross section and at a level that appears to replicate the

MiniBooNE cross section normalization. Whether such a model can also describe the kinematic distribution of the observed data remains to be seen. When this calculation is performed without multi particle-hole contributions (dashed black), the results are in agreement with the other impulse approximation results, as expected. The realization that nuclear effects can potentially increase the cross section is a revelation and a point to which we will return.

These surprising developments have not been evident in all experiments – the NOMAD experiment, operating at higher energy, measures results for both M_A and the QE cross section consistent with that expected from the historical value of M_A. However it should be noted that the experiments have differing criteria for what is termed a QE event. MiniBooNE selects events with a muon and no pions, while NOMAD selects events with only one (muon) or two (muon+proton) tracks. Thus, it is not clear how many events accepted by MiniBooNE are rejected by the NOMAD selection. The notion of what experimentally constitutes "the CCQE cross section" is hence somewhat subjective.

While it may be simply coincidental, the impulse approximation with a high M_A=1.35 GeV value appears to describe the low energy MiniBooNE data both in Q^2 shape and cross section normalization while the same is true for the high energy NOMAD data using the historical M_A=1.03 GeV value as input.

Quasi-Elastic Double Differential Cross Sections: Although much of the historical focus has centered on fitting observed Q^2 distributions to obtain M_A values and measuring total

cross sections as a function of neutrino energy, modern high statistics event samples have now allowed the first measurement of double-differential cross sections (26). Examining such double differential distributions can be especially illuminating in exposing underlying features in the data. As an example, measurement of $d^2\sigma/dT_\mu d\theta_\mu$ has revealed discrepancies (with respect to impulse approximation calculations) that tend along lines of constant Q^2 rather than E_ν. This suggests a mis-modeling of the underlying cross sections and not the incident neutrino flux predictions. Such measurements are useful in that they provide a more rigorous point of comparison and are much less model-dependent than extractions of M_A or cross sections as a function of derived quantities such as Q^2 and E_ν. To advance our understanding, future experiments should cross-compare differential cross sections measurements (and not model-dependent M_A values). Theoretical models should also aim to replicate such two-dimensional experimental distributions.

As we have seen, modern data has uncovered some unexpected discrepancies. What could be wrong? In the coming sections we will go back and critically evaluate some assumptions, explore differences between electro- and neutrino- nuclear scattering generally, delve further into the limitations of the impulse approximation approaches, as exposed in electro-nuclear scattering, and question the use of the term 'QE' when applied generically to data samples from experiments with very different detectors. The latter is particularly important as the impact FSI will have on a particular analysis depends critically on the details of the detector and experiment.

5. Electro-weak Scattering beyond the Impulse Approximation

The theoretical approach described in Section 3 was developed in the context of inclusive electo-nuclear QEES. Given the inability of this restricted approach to describe key features of recent neutrino-nucleus data, are there viable extensions that could achieve better agreement?

It is first worth pointing out several key differences between inclusive electro- and neutrino- nuclear scattering. In electron scattering, the incident flux and energy are precisely known; in neutrino scattering the flux is uncertain to 10-20% or more and the incident neutrino energy inferred from particles observed in the final state. Thus, there are large uncertainties on the kinematic quantities critical to describe neutrino QE scattering, in contrast to QEES inclusive electron scattering.

In inclusive QEES studies, the determination that an event is 'quasi-elastic' is based solely on leptonic variables. In neutrino scattering the final state of the hadronic system is always employed in event selection and often in reconstruction of the event kinematics. In contrast to the electron case, the determination that an event is QE is based on topology, necessarily involving hadronic information.

Extensions to the impulse approximation are presented below that may account for some of the effects noted in the experimental data. In particular could the QE cross section on ^{12}C exceed that of 6 free neutrons?

5.1 – Multi-Nucleon Correlations

QE scattering is traditionally viewed as scattering off single nucleons thus the hadronic electro-weak current is written as the sum of the individual nucleon one-body currents. The final hadronic state in this picture is a nucleon in the continuum and a "hole" in the recoiling target nucleus. The transferred energy from the leptonic sector to hadrons (ω) goes into creating the kinetic energy of the continuum nucleon plus the energy to create the "hole" in the recoiling A-1 nucleus.

This picture is attractive and readily calculable, but is too simple and quantitatively only good to tens of percent and in some instances off by more than factors of 2. Most of the disagreement is due to short-range forces between nucleons not accounted for in the average potential. When two nucleons are close to each other (r_{ij}<1.5 f) in spatially symmetric states [eg. T=0,S=1], strong short-range forces greatly increase their relative momentum and propel the two nucleons far off shell. Nuclear scientists have known about such short range correlations (SRCs) for some time but only recently (67,68) have direct evidence of their existence. These SRCs are found to be as theoretically expected (69,70) and a nucleon is involved in one about 20% of the time. These correlations mostly (90%) involve proton-neutron pairs with T=0, S=1. Their short-range tensor interaction produce

a 2p-2h fluctuation in the Fermi momentum distribution. The individual particle momenta involved in the fluctuation are well above the Fermi momentum as the pair can be several hundred MeV off shell. These correlations can be added to the Fermi momentum distribution as a perturbation or included in an RPA calculation. Of course, creating the nuclear ground state by solving the nuclear many-body problem with realistic nucleon-nucleon forces is preferable but with increasing complexity with increasing A, this procedure has been limited to$12 \geq A$.

There are existing calculations (66) that do account for such short-range correlations in neutrino scattering. The original aim (71) of this group was to account for ν-^{16}O "QE" interactions observed in a water Cherenkov detector viewing atmospheric neutrinos . Their point of view clearly extends the limitations imposed by the impulse approximation and consistently (66,71) produces appreciably larger cross sections than the more limited view following QEES . References (66) and (71) are carried out in RPA and incorporate both long and short-range correlations. Short-range correlations, principally the n-p isoscalar tensor interaction due to pion exchange produces 2p-2h configurations that considerably enhance the coupling to the transverse currents. This contribution is of course absent in the impulse approximation (one particle approach) as it arises from a two-particle correlation. There are some issues with respect to divergences that occur when integrating this contribution to the cross section over the momenta of the two correlated nucleons (72,73). Those problems with calculational issues aside, there is ample evidence that the transverse vector coupling is appreciably larger than predicted in the impulse approximation. As mentioned earlier, when separating the QEES response into its

longitudinal and transverse components, the longitudinal response has the expected magnitude, while the transverse response is as much as 50% larger than predicted by the impulse approximation. Both responses are normalized to be equal within the RFG impulse approximation (32,35). It is somewhat surprising that the large values associated with the transverse response has not received more attention as it's larger than expected yield has been evident for more than 20 years (72-74).

It is therefore perhaps no surprise that the neutrino QE cross section for ^{12}C is larger than predicted by the impulse approximation. However the measured cross section appears larger than that of 6 free neutrons. Note, this feature is captured in the calculation of (66,71) and one must inquire if such a large cross section is possible and if so how does it come about?

Some illumination regarding the possibility that the observed "quasi elastic" cross section exceed that for free nucleons can be found in an interesting calculation of the longitudinal and transverse response functions for QEES from ^{3}He and ^{4}He. This calculation is carried out in the framework of Euclidian Response Functions (32,77). The calculation has the drawback that it is non-relativistic but has the important advantage that it uses ground state wave functions calculated with realistic nucleon-nucleon forces so that all N-N correlations are present without their having to be perturbatively added to a simplified basis state.

The motivation for investigating ^{3}He and ^{4}He was the large change of the ratio of transverse to longitudinal response in observed in QEES. The larger size of the transverse

yield occurs even at ψ'=0, making it unlikely that it is due to the tail of the Δ resonance. Also, the non scaling above ψ'=1 for increasing momentum transfer is reminiscent of the behavior seen in the neutrino scattering experiments requiring large values for M_A. The formalism employed in (77) successfully accounts for all the features observed in the QEES on ^{3}He and ^{4}He.

Their approach calculates the longitudinal and transverse response functions employing ground state wave functions calculated with realistic N-N interactions. This work is part of a program that has been extremely successful (78) but of necessity limited to light nuclei (A<12). To calculate the response function the longitudinal and transverse vector currents impart 3-momentum $\vec{q}$ to the nuclear ground state. The Euclidian response is defined as an integral over the QE response

$$\hat{E}(|\vec{q}|,\tau) = \int_{\omega_{th}}^{\infty} e^{-(\omega - E_0)\tau} R_{T,L}(|\vec{q}|,\omega) d\omega \qquad (14)$$

where $R_{T,L}(|\vec{q}|,\omega)$ are the usual QEES responses, E_0 is the ground state energy of the target nucleus and ω_{th} is minimum energy of the final state excluding elastic scattering of the target. The quantity τ with dimension MeV^{-1} weights different intervals of final state energy. The value τ=0 is the integral over all final state energy and is the sum rule for each response function. The $\hat{E}_{L,T}$ are obtained from calculation as:

$$\hat{E}_L(|\vec{q}|,\tau) = \left\langle 0 \left| \rho(\vec{q})^* e^{-(H-E_0)\tau} \rho(\vec{q}) \right| 0 \right\rangle - e^{-\frac{q^2\tau}{2Am}} \left| \left\langle 0(\vec{q}) \left| \rho(\vec{q}) \right| 0 \right\rangle \right|^2 \qquad (15)$$

$$\hat{E}_T(|\vec{q}|,\tau) = \left\langle 0\left|\vec{j}_T(\vec{q})^* e^{-(H-E_0)\tau}\vec{j}_T(\vec{q})\right|0\right\rangle - e^{-\frac{q^2\tau}{2Am}}\left|\left\langle 0(\vec{q})\left|\vec{j}_T(\vec{q})\right|0\right\rangle\right|^2 \quad (16)$$

where the elastic scattering contributions are explicitly subtracted. The nuclear ground state wave function is $|0\rangle$ and $|0(\vec{q})\rangle$ is that ground state recoiling with momentum $\vec{q}$. The chief advantage of this approach is that it can be exactly calculated with final state interactions and two body currents. The ground states are solutions of a well tested Hamiltonian incorporating complex two body and three body nuclear interactions (78). The model has only nucleonic degrees of freedom but includes the effects of meson exchange via the continuity of the vector current (CVC).

$$div\ \vec{j} = \frac{\partial \rho}{\partial t} \quad (17)$$

which becomes

$$div\ \vec{j} = [H, \rho] \quad (18)$$

The various short-range, two body forces present in the Hamiltonian require meson exchange to be incorporated into the transverse vector current. Far and away the most important of these short range correlations is again the tensor force due to pions. Reference (75) demonstrated that the effect of including <u>both</u> short range correlations and two body currents greatly increases the transverse response. Results presented in reference (77) show the greatly enhanced strength (~50%) resulting from meson exchange using a properly correlated ground state versus much smaller enhancement (7%) for a Fermi Gas approach. The enhancement obtained in (77) is sufficient to show that the correlations and 2-body currents can produce a response in excess of that of free nucleons. Reference (77)

shows that a large fraction of the increased transverse strength occurs for $\tau<0.01$ which roughly corresponds to $\omega > 100$MeV. This would push such events into the tail of the Δ resonance and they would not be counted in inclusive QEES.

Thus, this calculation appears to confirm the notion that a broader definition of QE scattering allows the cross section for

$$\nu_l + (N,Z)_0 \rightarrow l^- + N-1, Z+1$$

to exceed the cross section for

$$N(\nu_l + n \rightarrow l^- + p)$$

This approach may soon be extended to neutrino scattering (79). It will be interesting to see the results.

Reference (80) examined the results of (26,29) and incorporated meson exchange currents into their calculation. Their calculation fails most seriously for larger angles ($\theta > 45^0$) where the transverse contributions become dominant. Including meson exchange improves the disagreement with data but not sufficiently. As this calculation is carried out using super-scaling (35,32) explicit short-range correlations are not included so a short fall could be expected. This work has been extended to QEES (73) including short-range correlations but this more extensive approach has not yet been applied to neutrino CCQE.

5.2 – Final State Interactions

Characterizing a neutrino nucleus interaction often depends on the hadronic final state. This final state can be modified by what are termed final state interactions (FSI). The definition of FSIs is somewhat arbitrary but in general can be understood as a subsequent strong interaction of the product of the electroweak vertex with the other nucleons in the nucleus.

The prevalence of final state interactions can be estimated by calculating a mean free path for scattering (λ) of the struck nucleon

$$\lambda = \frac{1}{\sigma n} \qquad (19)$$

where n is the number of nucleons per cm^3 and σ is a characteristic N-N scattering cross section with $n = 1/(7.24 \times 10^{-39})$ and $\sigma = 40 \times 10^{-27}$, $\lambda = 1.8 \times 10^{-13}$ cm. Fortunately the situation is not that bad, the repulsive part of the N-N interaction gives the struck nucleon a "free ride" for $\sim .6 \times 10^{-13}$ cm. Though FSI often play a key role in understanding particular reactions, little experimental work has been done in this area. Carrying out meaningful measurements requires preparing a well defined initial state in the nucleus and a measurement of the final products. Reactions of (e,e',p) where the initial state is created by conventional quasielastic scattering off a proton have been examined in ^{12}C, ^{27}Al, ^{58}Ni and ^{181}Ta with the proton recoil energy averaging 180 MeV (81). There appears to be a fair theoretical characterization of the fate of struck proton in these cases (82). Proton recoil energies up to 1.8 GeV have been examined in (83). Ongoing studies at Jefferson Laboratory (84) in e-^{3}He scattering finds that the unfolding of initial and final state interactions is more

complicated in collisions where short range correlations are involved. This will likely be the case for many of the events occurring in neutrino-nucleus scattering.

Given the difficulty of calculating the myriad possible final states it appears that a well-planned investigation of FSI with electron beams will be needed to quantitatively clarify their role.

6. Conclusions

6.1 – What is 'Quasi-Elastic' Scattering?

Results from modern neutrino experiments have provided some cautionary tales. Neutrino QE scattering from nuclei appears more complicated than previously envisioned. There are complex nuclear effects in play that, as we have seen, can increase cross sections and produce more complicated final states. Hence, some care must be taken in defining a neutrino QE interaction. Experiments measuring a more inclusive final state may obtain higher yields than those requiring a strict muon and single proton final state. This should serve as word of warning to future oscillation experiments that use fine-grained near detectors to measure "quasi-elastic" cross sections using muon+proton samples and then apply that constraint to predict "quasi-elastic" events in a less-capable far detector whose definition would be more inclusive because an outgoing proton track cannot be detected.

To make progress, what is clearly needed is a reconciliation between calculation and experiment in what has been term QE scattering. It is likely that much of the disagreement between existing experimental measurements and between the calculation of QE scattering and the observed data is due to differing constraints applied in each case. Most of the calculations are restricted to the impulse approximation applied to a momentum distribution of individual nucleons. At the same time, experimental selection that is more inclusive in what is termed QE will include all of the enhancements expected from meson exchange and short-range correlations, effects that are absent in impulse approximation calculations that impose kinematic constraints suitable to inclusive QEES. So it may be that different QE definitions lead to fundamentally different results. With careful investigation, this explanation may be probed by the next generation of theoretical calculations and experimental investigation.

6.2 – Future Directions

Even if the conjectures mentioned above are correct, severe challenges for the theoretical program remain. Among the most serious is how to treat the interference between vector and axial vector amplitudes in the transverse response. The interference effects between the transverse vector and axial vector amplitudes are far from obvious and may be further complicated by FSI. Thus the results of (66,75) while employing reasonable parameters and agreeing with the observed cross sections as a function of neutrino (anti-neutrino) data leave some open questions. Are the effects of short-range correlations on the axial currents as small as previously estimated? A more proper treatment of their effect on the

transverse vector response shows a much larger (77) impact than simpler estimates. What happens when relativistic effects are more fully respected? If a quantitatively robust description of neutrino-nucleus scattering is achieved, how will its content be incorporated into neutrino event generators? Once implemented, can these models explain the double-differential distributions in the data (and not just the cross section as a function of neutrino energy)?

Future experiments also have an important role to play. A very significant program of looking at the relationship between, short-range correlations, meson exchange currents, and FSI in electron scattering from ^{3}He is underway (84) at Jefferson Laboratory. The initial results appear far from simple to understand even for such a light nucleus.

There are also implications and opportunities for future neutrino experiments (85). Next generation neutrino experiments will have event samples in the millions, and to obtain precise results, improved accuracy on the largest systematic – the flux – will be crucial. Dedicated hadroproduction measurements (86) and more extensive monitoring of beam muons, will play a key role (59). Experiments such as Minerva and the T2K Near Detectors will be able to study neutrino scattering using targets over a range of nuclei from helium to lead in the same beam, collect data with neutrinos and antineutrinos, and have high efficiency for two-track selection over a wide range of Q^2 and neutrino energy. Future liquid argon detectors, being strongly affected by nuclear effects, will have extremely low energy thresholds for detection of all particles produced in the interactions, particularly

multiple nucleons which would be the 'smoking gun' for the np-nh explanations discussed previously. An improved understanding of nuclear effects, of course, will be needed if these detectors are to reach their full potential for physics measurements.

Overally, it is quite exciting that the study of neutrino QE scattering has opened such questions. Such a seemingly mundane topic is far from that. Together, dedicated theoretical and experimental work on this important topic will help clarify the issues raised by modern data and propel us into the future.

Acknowledgements: The work of one author (HG) was supported by DOE grant DE-FG02-92ER40702. We would like to thank L. Alvarez-Ruso, O. Benhar, W. Donnelly, J. Nieves, J. Sobczyk, and R. Tayloe for numerous helpful conversations. We also gratefully acknowledge the assistance of C. Andreopoulos, J. Carlson, S. Dytman, R. Gran, T. Katori, J. Nowak, and H. Tanaka with specific items in this paper.

Literature Cited:

1. Llewellyn-Smith CH. *Physics Reports* 3:261 (1972)
2. M. Holder et al. *Nuovo Cim.* 57A: 338 (1968)
3. Kustom RL. *Phys. Rev. Lett.* 22: 1014 (1969)
4. Block MM et al. *Phys. Lett.* 12: 281 (1964); Orkin-Lecourtis A et al, *Nuovo Cim.* 50A: 927 (1967); Budagov T et al, *Phys. Lett.* 29B: 524 (1969); *Nuovo Cim.* 2: 689 (1969)
5. Singh SK. *Nucl. Phys.* 36B: 419 (1972)
6. Amsler C et al (Particle Data Group). *Phys. Lett.* 667B: 1 (2008)
7. Lyubushkin V et al. *Eur. Phys. J*. 63C:355 (2009)
8. Singh SK, Oset E. Nucl. Phys. 542A:587 (1992)
9. Bernard V et al. *J. Phys.* 28G:R1 (2002)
10. Budd H, Bodek A, Arrington J. *Nucl. Phys. Proc. Suppl.* 139:90 (2005)
11. Bodek A, Avvakumov S, Bradford R, Budd H. arXiv:0709.3538 [hep-ex]
12. Kuzmin KS, Lyubushkin VV, Naumov, VA. arXiv:0712.4384v3 [hep-ph]
13. W.A. Mann et al. *Phys. Rev. Lett.* 31: 844 (1973); Miller KL et al. *Phys. Rev.* 26D:537 (1982)
14. Barish SJ. *Phys. Rev.* 16D:3103 (1977) (was anl-flux)
15. Allasia D. *Nucl. Phys.* 343B:285 (1990)
16. Baker NJ et al. *Phys. Rev.* 23D:2499 (1981); Fanourakis G et al. *Phys. Rev.* 21D:562 (1980)
17. Kitagaki T et al. *Phys. Rev.* 28D:436 (1983); Asratyan AE et al. *Sov. J. Nucl. Phys.* 39:392 (1984)

18. Budagov I et al. Lett. *Nuovo Cim.* 2:689 (1969); Bonetti S et al. *Nuovo Cim.* 38A:260 (1977); Armenise N et al. *Nucl. Phys.* 152B:365 (1979); Pohl M et al. *Lett. Nuovo Cim.* 26:332 (1979)
19. Belkov SV et al. *Z. Phys.* 320A:625 (1985)
20. Grabosch HJ et al. *Sov. J. Nucl. Phys.* 47:1032 (1988); Brunner J et al. *Z. Phys.* 45C:551 (1990); Ammosov VV et al. *Sov. J. Part. Nucl.* 23:283 (1992)
21. Antonello M. *AIP Conference Proceedings* 1189:88 (2009)
22. Gran R et al. *Phys. Rev.* 74D:052002 (2006)
23. Soderberg M. *AIP Conference Proceedings* 1189:83 (2009)
24. Drakoulakos D et al. arXiv:0405002 [hep-ex] (2004)
25. Aguilar-Arevalo AA et al. *Phys. Rev. Lett.* 100:032301 (2008)
26. Aguilar-Arevalo AA et al. *Phys. Rev.* 81D:092005 (2010)
27. Dorman M. *AIP Conference Proceedings* 1189:133 (2009)
28. Djurcic Z. *AIP Conference Proceedings - NuFact10* (2011)
29. Alcaraz-Aunion JL, Walding J. *AIP Conference Proceedings* 1189:145 (2009)
30. Ferrero A. *AIP Conference Proceedings* 1189:77 (2009)
31. Day D. 2007. *Quaisielastic Electon Nucleus Scattering Archive*. http://faculty.virginia.edu/qes-archive
32. Benhar O, Day D, Sick I. *Rev of Mod. Phys.* 80:189 (2008)
33. Walecka JD. *Electron Scattering for Nuclear and Nucleon Structure*, Cambridge MonoGraphs on Particle Physics, Nuclear Physics, and Cosmology ed. y T. Ericson and P.V. Landshoff.
34. Czyz W, Gottfried K. *Ann. Phys.(N.Y.)* 21:47 (1963)
35. DeForest T, Walecka JD. *Ann. Phys.(N.Y.)* 28: 18 (1964)

36. Moniz EJ. *Phys. Rev.* 184:1154 (1969)

37. Moniz EJ et al. *Phys. Rev. Lett.* 26:445 (1971)

38. Benhar O et al. *Nucl. Phys.* 579A:493 (1994)

39. Sick I, Day E, McCarthy J. *Phys. Rev. Lett.* 45:871 (1980)

40. Sick I. *Proceeding of the Conference on Weak and Electromagnetic Interactions in Nuclei* edited by H.V. Klapdor (1986)

41. Alberico WM et al. *Phys. Rev.* 38C:1801 (1988)

42. Donnelly TW, Sick I. *Phys. Rev.* 60C:065502 (1999)

43. Jourdan J. *Nucl. Phys.* 603A:117 (1996)

44. Amaro JE et al. *Phys. Rev.* 71C:015501 (2005)

45. Benhar O et al. *Phys. Rev.* 72C:053005 (2005); Benhar O, Meloni D. *Nucl. Phys.* 789A:379 (2007)

46. Leitner T, Alvarez-Ruso L, Mosel U. *Phys. Rev.* 73C:065502 (2006)

47. Ankowski AM, Sobczyk JT. *Phys. Rev.* 77C: 044311 (2008)

48. Nieves J, Valverde M, Vincente-Vacas MJ. *Phys. Rev.* 73C:025501 (2006)

49. Ahrens LA et al. *Phys. Rev.* 34D:75 (1986)

50. Kitagaki T et al. *Phys. Rev. Lett*. 49:98 (1982)

51. Orkin-Lecourtois A, Piketty CA. *Nuovo Cimento* 4:927 (1967)

52. Ahn MH et al. *Phys. Rev.* 74D:072003 (2006)

53. Aguilar-Arevalo AA et al. *Phys. Rev.* 79D:072002 (2009)

54. Butkevich AV. *Phys. Rev.* 78C:015501 (2008)

55. Leitner T, Mosel U. *Phys. Rev.* 81C:064614 (2010)

56. Smith R, Moniz E. *Nucl. Phys.* 43B:605 (1972). Erratum-ibid 101B:547 (1975)

57. Bodek A, Ritchie J. *Phys. Rev.* 23D:1070 (1981)

58. Dytman S. *AIP Conference Proceedings* 1189:51 (2009)

59. Kopp S. *Phys. Rept.* 439:101 (2007)

60. Benhar O, Coletti P, Meloni D. arXiv:1006.4783 [nucl-th] (2010); Benhar O. arXiv: 1012.2032 [nucl-th] (2010)

61. Butkevich AV, *Phys. Rev.* 80C:014610 (2009)

62. Athar MS et al. arXiv:0908.1443 [nucl-th] (2009)

63. Maieron C et al. *Phys. Rev.* 68C: 048501 (2003)

64. Jachowicz N et al. *Nucl. Phys. Proc. Suppl.* 155:260 (2006), Jachowicz N et al. *Phys. Rev.* 76C:055501 (2007)

65. Dytman S. *AIP Conference Proceedings* 1189:60 (2009)

66. Martini M et al. *Phys. Rev.* 80C:065501 (2009)

67. Egiyan K et al. *Phys. Rev. Lett.* 96:082501 (2006)

68. Shneor R et al. *Phys. Rev. Lett.* 99:072501 (2007)

69. Sargsian MM et al. *Phys. Rev.* 71C:044615 (2005)

70. Schiavilla R et al. *Phys. Rev. Lett.* 98:132501 (2007)

71. Marteau J, Delorme J, Ericson M. *Nucl .Inst. Meth.* 451A:76 (2000)

72. Davesne D et al. *Phys. Rev.* 80C:024314 (2009)

73. Amaro JE et al. *Phys. Rev.* 82C:044601 (2010)

74. Finn J, Lourie RW, Cottmann BH. *Phys. Rev.* 29C:2230 (1984)

75. Martini M et al. *Phys Rev.* 81C:045502 (2010)

76. Zeller G. private communication

77. Carlson J et al. *Phys. Rev.* 65C:024002 (2002)

78. Wiringa RB et al. *Phys Rev.* 63C:017603 (2000)

79. Carlson J. private communication

80. Amaro JE et al. arXiv:1010.1708 [nucl-th] (2010)

81. Garino G et al. *Phys. Rev.* 45C:780 (1992)

82. Pandharipande V, Peiper S. *Phys. Rev.* 45C:791 (1992)

83. Abbot D et al. *Phys. Rev. Lett.* 80:5027 (1998)

84. Weinstein L. *Presented at HENP and QCD*, Feb 6-9, Miami 2010

85. Alvarez-Ruso L et al. *AIP Conference Proceedings* 1189:291 (2009)

86. Popov B. *AIP Conference Proceedings* 1189:97 (2009)

Article Components:

Abstract: The study of neutrino oscillations has produced a new generation of neutrino experiments that are also exploring neutrino-nuclear scattering processes. We focus in particular on charged current quasi-elastic scattering, a particularly important channel that has been extensively investigated both in the bubble chamber era and by the current generation of experiments. These recent results have created theoretical reexamination of the issue. In this paper we will review the standard picture of quasi-elastic scattering as developed in electron scattering, review and discuss experimental results, and discuss additional nuclear effects such as exchange currents and short range correlations that may be playing a significant role in neutrino-nucleus scattering.

Key Terms:

Neutrino Charged Current Quasi-Elastic Scattering - On free nucleons, the process $\nu_\mu n \to \mu^- p$ and $\bar{\nu}_\mu p \to \mu^+ n$. The largest neutrino scattering cross section at 1 GeV and the focus of this review article.

Final State Interactions – Reinteraction of hadrons produced in the neutrino scattering process with the spectator nucleus. Delta production, followed by pion reabsorption, is a particularly important example.

Relativistic Fermi Gas - The simplest impulse approximation approach where the nucleus is treated as a degenerate Fermi Gas.

Impulse Approximation – An approach to lepton-nucleus scattering where the scattering cross section is calculated as the incoherent sum of scattering from free nucleons with some initial momentum and energy distribution.

Spectral Functions – $S(\vec{p},E)$, which gives the probability of finding a nucleon with momentum $\vec{p}$ and removal energy E, and includes a high-momentum tail in an attempt to account for short-range nucleon-nucleon correlations.

Quasi-Elastic Electron Scattering - Electron scattering in the kinematic regime dominated by single-nucleon knockout, and where the impulse approximation approaches are highly successful in describing data.

Nucleon-nucleon correlations: Scattering processes that are sensitive to correlations between the wavefunctions of two or more nucleons. Scattering from a quasi-deuteron in the nucleus would be an example of a short-range correlation.

Acronyms:

CCQE – Charged Current Quasi-Elastic
CVC – Conserved Vector Current
FSI – Final State Interactions
IA – Impulse Approximation
PCAC – Partially Conserved Axial Current
QE – Quasi-Elastic
QEES – Quasi-Elastic Electron Scattering
RFG – Relativistic Fermi Gas
RPA – Random Phase Approximation
SRC – Short Range Correlations

Summary Points:

1. An improved understanding of neutrino-nucleus interactions will be important for future oscillation experiments.

2. There is an apparent inconsistency between the old (mainly bubble chamber, light targets) and new (electronic detectors, nuclear targets) generation of neutrino quasi-elastic scattering measurements.

3. The Impulse Approximation has been extremely successful at describing electron scattering over a wide range of kinematics where the kinematic conditions of the calculation are respected.

4. There are fundamental differences in the electro- and neutrino-nuclear contexts, in particular the relatively poor knowledge of the flux and neutrino energy in neutrino experiments.

5. Certain nuclear effects, such as multi-nucleon correlations and final state interactions, play a much larger role in neutrino data sets than they do in electron scattering studies, which have the luxury of being able to restrict kinematics.

6. Data collected in the most recent neutrino experiments on nuclei including carbon, oxygen, and iron, have turned up several intriguing results which are inconsistent with those from the bubble chamber era.

7. When comparing data to calculation it is crucial that the two be matched to incorporate all final states (including multi-nucleon states) that could be present in the data.

Future Directions:

1. It is crucial to understand how the measured cross section on ^{12}C at ~1 GeV could exceed that for 6 free neutrons.
2. A new generation of high-precision experiments will be probing these questions in the coming decade.
3. How well will future experiments be able to improve their understanding of the flux, which is the limiting systematic error in most of these measurements?
4. Care will need to be taken by future experiments to ensure that the calculations match the experimental conditions.

5. It will be interesting to see how calculations involving multi-nucleon correlations including meson exchange currents match recent results in cross section normalization and Q^2 shape.
6. Direct measurement of multi-nucleon final states in a neutrino detector with low thresholds could play an important role in quantifying scattering from correlated nucleon states.

Figure Captions:

Figure 1*: The diagram on the right is the most commonly employed model of QE neutrino scattering. The nucleus is treated as a collection of independent nucleons. The neutrino- nucleon interaction, both charged (ν,μ) and neutral (ν,ν), is assumed to be impulsive with the spectator nucleons remaining in their initial states. The diagram on the left is meant to show the complexity of the real situation where the interaction need not place on a nucleon given the presence of short range interactions between nucleons.*

Figure 1: *Idealized spectrum of few GeV electrons scattered off a nucleus at fixed scattering angle (modified from [cite:BenharReview]). The horizontal axis is the energy lost by the electron in the scattering. The labels indicate the individual contributions to the total yield.*

Figure 3*: a) Inclusive electron scattering spectra on ^{3}He taken at widely different incident energies and scattering angles. Note the incident energies differ by factors of almost 25 while the cross sections differ by over 10^3. b) Similar data plotted as a function of the scaling variable y. See ref [cite:BenharReview] for further details.*

Figure 4*: Quasi-elastic scattering results. A) Total cross section measurements, B) MiniBooNE Q^2 distribution [cite: data-miniboone-prl]. Dotted line indicates predicted non-quasi-elastic backgrounds to the sample. The dashed line is the prediction using the nuclear model of Reference [smith-moniz] with M_A=1.03 GeV. The solid line is a shape-only fit to the data assuming a higher M_A value.*

Tables:

Experiment	$<E_\nu>$	Target	Detector	Year	References
ANL	0.5 GeV	Fe, D_2	spark chamber, bubble chamber	1969-1982	(2,13,14)
BEBC	54 GeV	D_2	bubble chamber	1990	(15)
BNL	1.6 GeV	D_2, H_2	bubble chamber	1980-1981	(16)
FNAL	27 GeV	D_2, Ne-H_2	bubble chamber	1982-1984	(17)
GGM	2.2 GeV	C_3H_8, CF_3Br	bubble chamber	1964-1979	(18)
Serpukhov	3-30 GeV	Al	spark chamber	1985	(19)
SKAT	9 GeV	CF_3Br	bubble chamber	1988-1992	(20)
ArgoNeuT	3.3 GeV	Ar	Liquid argon TPC	2009-2010	(21)
K2K	1.3 GeV	CH_2, H_2O	Tracking detectors – solid scintillator strips + scintillating fiber tracker	2003-2004	(22)
MicroBooNE	0.8 GeV	Ar	Liquid argon TPC	2013+	(23)
MINERvA	3.3 GeV	C, Fe, Pb	Tracking detector (solid scintillator strips) + EM and hadronic calorimetery	2009+	(24)
MiniBooNE	0.8 GeV	CH_2	Cerenkov detector	2002+	(25,26)
MINOS	3.3 GeV	Fe	Tracking calorimeter – iron plates + solid scintillator strips	2004+	(27)
NOMAD	26 GeV	C	Drift chambers	1995-1998	(7)
NOvA ND	2 GeV	CH_2	Tracking detector – liquid scintillator cells	2010+	(28)
SciBooNE	0.8 GeV	CH	Tracking detector (solid scintillator strips)+ EM calorimeter	2007-2008	(29)
T2K ND	2.1 GeV	C, H_20	Tracking detectors – solid scintillator + TPCs + EM calorimeters	2010+	(30)

Table 1: *Attributes of experiments that have measured neutrino quasi-elastic scattering processes or that will complete such studies in the near future. Bubble chamber era experiments are listed at the top, more recent experiments at the bottom. Mean energies for FermiLab NuMI experiments MINOS, MINERvA, and ArgoNeuT are for the Low Energy beam configuration.*

Experiment	**Selection**	**# Events**	**QE Purity**	**Flux/ Reference**	M_A	$F_A(Q^2)$	$\sigma(E_\nu)$	$\frac{d\sigma}{dQ^2}$	$\frac{d^2\sigma}{dT_\mu d\theta_\mu}$
ANL	2 and 3-track	1,737	98%	Hadro (14)	√		√	√	
BEBC	3-track	552	99%	ν_μ CC (15)	√		√	√	
BNL	ν : 3-track $\bar{\nu}$: 1-track	ν : 1,138 $\bar{\nu}$: 13	ν : 97% $\bar{\nu}$: 76%	ν_μ QE (49)	√		√		
FNAL	ν : 2 and 3-track $\bar{\nu}$: 1-track	ν : 362 $\bar{\nu}$: 405	ν : 97% $\bar{\nu}$: 85%	ν_μ QE (50)	√		√		
GGM	ν : 2-track $\bar{\nu}$: 1-track	ν : 337 $\bar{\nu}$: 837	ν : 97% $\bar{\nu}$: 90%	Hadro (51)	√	√	√	√	
Serpukhov	1-track	ν : 757 $\bar{\nu}$: 389	ν : 51% $\bar{\nu}$: 54%	Hadro, ν_μ CC (19)	√	√	√		
SKAT	ν : 2-track $\bar{\nu}$: 1-track	ν : 540 $\bar{\nu}$: 159	N/A	ν_μ CC (20)	√		√	√	
K2K	1 and 2 track	5,568	62%	Hadro, ν_μ CC (52)	√				
MiniBooNE	1-track	146,070	77%	Hadro (53)	√		√	√	√
SciBooNE (preliminary)	1 and 2-track	16,501	67%	Hadro (53)			√		
MINOS (preliminary)	1 track	345,000	61%	ν_μ CC (27)	√				
NOMAD	ν : 1 and 2-track $\bar{\nu}$: 1-track	ν : 14,021 $\bar{\nu}$: 2,237	ν :42% / 74% $\bar{\nu}$: 37%	Hadro, DIS, IMD (7)	√		√		

***Table 2**: Summary of analysis techniques employed in the experimental study of neutrino quasi-elastic scattering.*

Figures:

Figure 1:

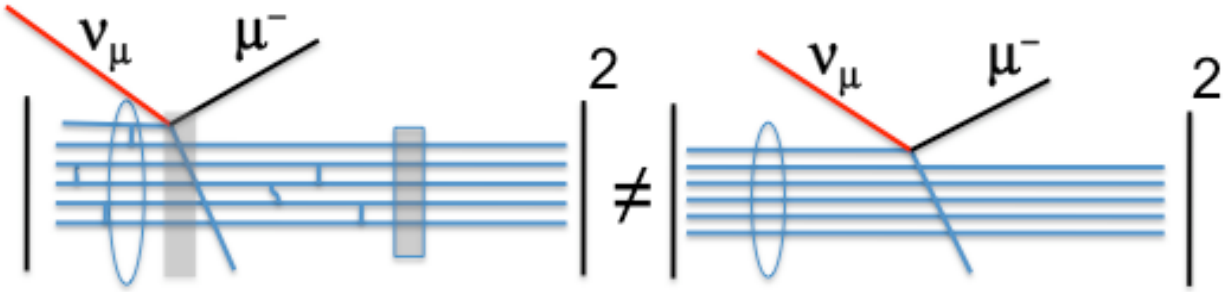

Figure 2:

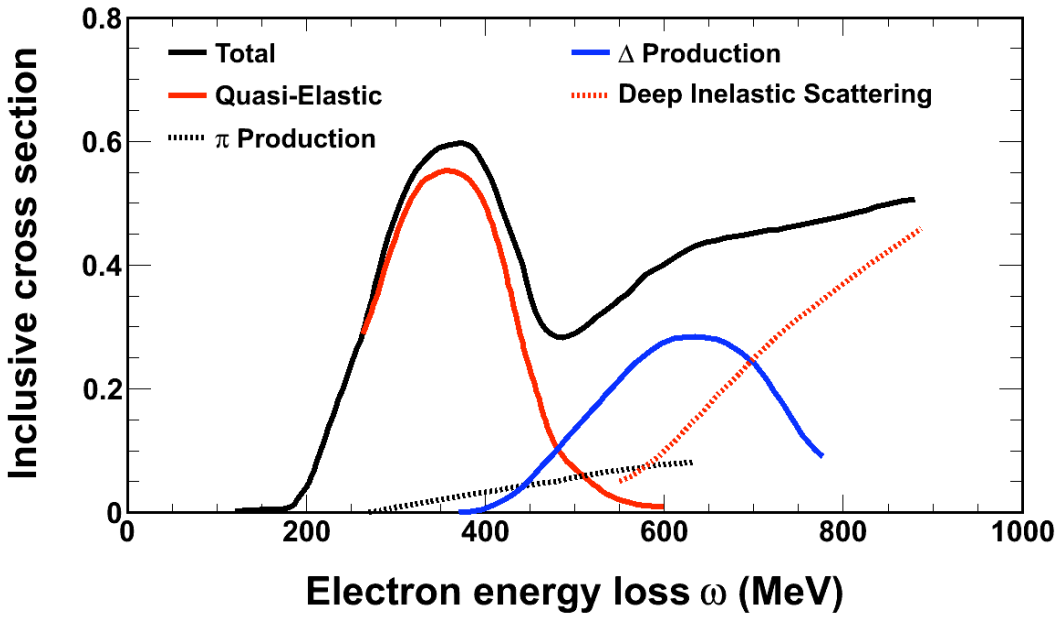

Figure 3:

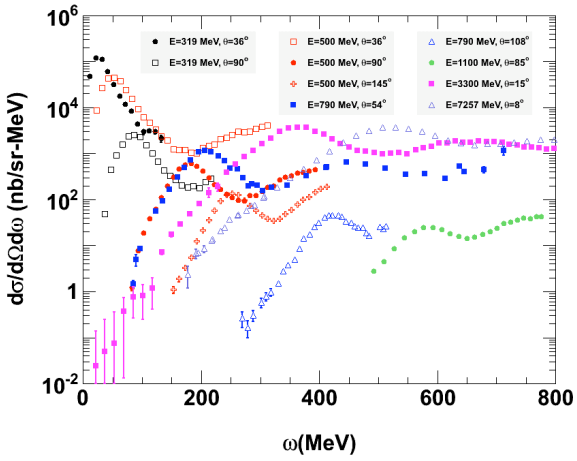
E=319 MeV, θ=36°
E=319 MeV, θ=90°
E=500 MeV, θ=36°
E=500 MeV, θ=90°
E=500 MeV, θ=145°
E=790 MeV, θ=54°
E=790 MeV, θ=108°
E=1100 MeV, θ=85°
E=3300 MeV, θ=15°
E=7257 MeV, θ=8°
dσ/dΩdω (nb/sr-MeV)
ω(MeV)

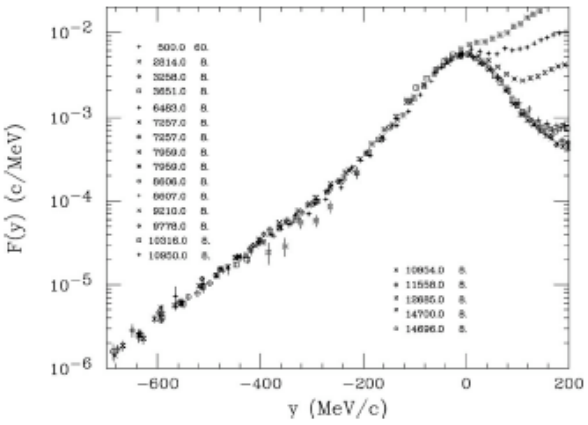
F(y) (c/MeV)
y (MeV/c)

Figure 4:

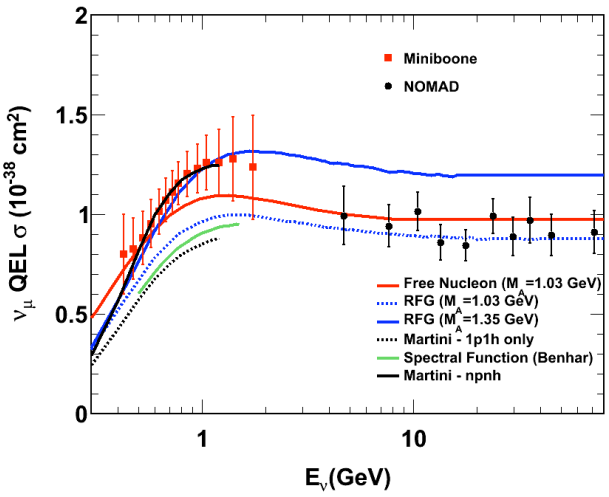
Miniboone
NOMAD
Free Nucleon (M_A=1.03 GeV)
RFG (M_A=1.03 GeV)
RFG (M_A=1.35 GeV)
Martini - 1p1h only
Spectral Function (Benhar)
Martini - npnh
ν_μ QEL σ (10^-38 cm^2)
E_ν(GeV)

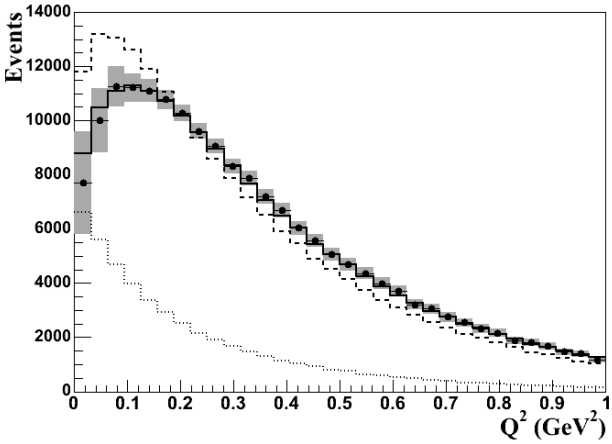
Events
Q² (GeV²)